ARMY RESEARCH LABORATORY

Fluorescence Image of a Single Molecule in a Microsphere: Model

Steven C. Hill, Paul Nachman, Stephen Arnold, J. Michael Ramsey, and Michael D. Barnes

ARL-TR-1979 July 1999

The findings in this report are not to be construed as an official Department of the Army position unless so designated by other authorized documents.

Citation of manufacturer's or trade names does not constitute an official endorsement or approval of the use thereof.

Destroy this report when it is no longer needed. Do not return it to the originator.

Army Research Laboratory

Adelphi, MD 20783-1197

ARL-TR-1979 **July 1999**

Fluorescence Image of a Single Molecule in a Microsphere: Model

Steven C. Hill

Information Science and Technology Directorate, ARL

Paul Nachman

TRW, Inc.

Stephen Arnold

Microparticle Photophysics Laboratory

J. Michael Ramsey and Michael D. Barnes

Oak Ridge National Laboratory

Abstract

We model fluorescence images of single molecules in spherical dielectric microcavities. Molecules are treated as time-harmonic dipoles. Images are integrated over emission frequencies. Because of the strong refractive properties of the enclosing sphere, the fluorescence image depends on the refractive index of the sphere and the position, orientation, and emission frequency of the molecule. When the dipole's emission is at the frequency of a microsphere resonance, the brightest regions in the images appear to originate from outside the sphere for some dipole positions. This type of calculation should help in interpreting images of molecules in microspheres.

Contents

Figures

1. Introduction

Images of fluorescence from single molecules in a gel [1], at a polymer-air interface [2,3], and on the surface of a poly(acrylamide) matrix [3] have been used to investigate a variety of photophysical phenomena. Images of a single molecule excited by the resonant fields outside a 2-mm-diameter sphere have been used to measure the absorption linewidths of molecules at low temperature [4]. Recently, images of the fluorescence from single molecules inside dielectric microspheres 7 to 9 μm in diameter have been reported [5]. Modeling single-molecule fluorescence images embedded in microspheres is the primary emphasis of this report.

Our method and results are also relevant to images of droplets containing many emitting molecules. Images of inelastic emission (lasing [6], stimulated Raman scattering [7], and fluorescence [8–11]) from multiple molecules in spheres and perturbed spheres have been used to investigate modal energy distributions, orientations [8], and lifetimes [12] of molecules at the surfaces of spheres [8], energy transfer between molecules in spheres [9], and internal circulation in droplets [10,11].

Prior calculations of images from microspheres have mostly treated elastic scattering: computed one-dimensional [13–16] and two-dimensional [17] images of the elastic scattering by spheres have been reported and compared with experiment [15–17]. Prior calculations of fluorescence images from spheres have employed geometrical optics: fluorescence images of relatively large droplets (5 mm diameter [11] or 400 μm diameter [18]), illuminated with laser beams focused along an equatorial plane of a droplet [11,18], have been simulated and restored using geometrical optics, which appears to be adequate for modeling images of the droplets used in these combustion studies (with diameters greater than 200 μm). However, because of the importance of diffraction by the sphere, including morphology-dependent resonances (MDRs, or whispering gallery mode resonances [19]), geometrical optics is, in many cases, inadequate for interpreting inelastic-emission images of smaller spheres. This is particularly true when gain processes are supported by MDRs [6,7] or when the microspheres are in a size range (say, 1 to 15 μm diameter) where cavity mode effects on spontaneous emission rates [12,20,21] are important, and where single-molecule fluorescence is studied [22,23]. Single-, nonresonant-frequency images calculated using physical optics have been presented previously in a paper

[5] that emphasized experimental work, but few details of the model or method of calculation were presented.

We describe here a physical optics method of calculating the image of a single emitting molecule inside a microsphere. The emission from the molecule, modeled as a dipole, is expanded in the vector spherical harmonics [24,25]. Our method includes integration over the fluorescence linewidth of the emitting molecule. Because we do not make either a Fresnel or paraxial approximation in computing the images, and *do* include the vector nature of the fields, our method is not restricted to images obtained with low numerical aperture (NA) systems as was the case for previously reported calculated elastic-scattering images [15–17]. Here we present calculated images for single-frequency emission, both on and off resonances of the sphere, and frequency-integrated images. The images depend on parameters such as the radius (a) and refractive index (m) of the sphere, position and orientation of the dipole, emission wavelength (and whether this is near a resonance of the sphere), and the NA of the lens. With a single dipole in the sphere, resonant emission may appear to emanate from outside the sphere, multiple regions of the sphere may appear bright (with the brightest spots in the image appearing opposite where they would be if the sphere were not there), or a spot may appear large and distorted. Because of the interest in oriented molecules near the surface of a microsphere [12], and because it has been shown that single molecules near the surface can be spatially photoselected [22], we emphasize molecules near the microsphere surface.

Calculations such as these should help in determining the extent to which the position and orientation of a single molecule in or on a microsphere can be determined from fluorescence images, and should be useful in interpreting images of inelastic emission from spheres containing multiple emitting molecules.

2. Model and Methods

The problem is illustrated in figure 1. The main assumptions we make in our model follow: The sphere is homogeneous (except for the single molecule), perfectly spherical, and sufficiently far from other objects (including the lens) that the problem is that of a sphere in an infinite medium. The molecule's natural emission lineshape is Lorentzian. The molecule does not reabsorb its emission. The molecule's emission at each frequency can be modeled as that from a time-harmonic dipole. The lens (or system of lenses) is diffraction limited, i.e., it converts diverging spherical waves S_1 into converging spherical waves S_2 [26]. The fields that excite the molecule are filtered out of the image. (The exciting fields are not specified; we begin with an excited molecule.) With these assumptions the image can be obtained using physical optics, as described in the next sections.

2.1 Green Function for Source Inside Sphere

When a polarization source $\mathbf{p}(\mathbf{r}')$ (at source point $\mathbf{r}'$ inside the sphere) radiates, additional fields are induced inside and outside the sphere so that the tangential components of the electric and magnetic fields are matched at the sphere surface [24]. The resulting electric fields at field point $\mathbf{r}$ outside

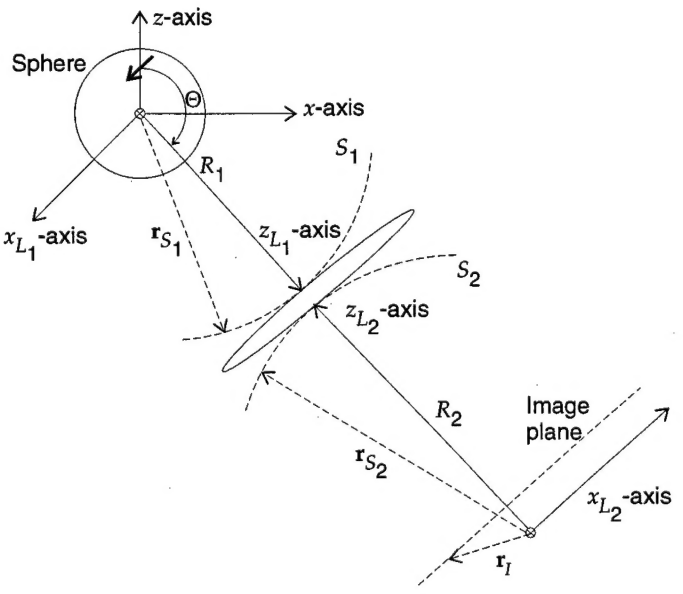

Figure 1. Diagram in $y = 0$ plane showing sphere, dipole, lens, and axes. y-axis points into page in all three coordinate systems. Lens converts diverging spherical wave on S_1 into converging spherical wave on S_2. Dipole is always on z-axis of sphere/dipole system. Image is centered on z_{L_2} axis.

the sphere can be written as a dyadic Green function (using a common notation for vector spherical harmonics from light-scattering work [27,28,25]) as*

$$\mathbf{E}^{\mathrm{s}}(k\mathbf{r}) = \frac{i\omega^2\mu k\mathrm{m}}{\pi}\sum_{\nu=1}^{\infty} D_\nu[\eta_n^{TE}\mathbf{M}_\nu^3(k\mathbf{r})\mathbf{M}_\nu^1(\mathrm{m}k\mathbf{r}') + \eta_n^{TM}\mathbf{N}_\nu^3(k\mathbf{r})\mathbf{N}_\nu^1(\mathrm{m}k\mathbf{r}')]\ \mathbf{p}(\mathbf{r}'), \tag{1}$$

where $k = 2\pi/\lambda$ is the wave number; λ is the free-space wavelength; ω is the radian frequency [$\exp(-i\omega t)$ time variation]; m in Roman script is the complex index of refraction; $\mathbf{M}_\nu^1$ and $\mathbf{N}_\nu^1$, and $\mathbf{M}_\nu^3$ and $\mathbf{N}_\nu^3$, are the vector spherical harmonic functions of the first and third kind, respectively (for $\mathbf{M}_\nu^3$ and $\mathbf{N}_\nu^3$, the spherical Bessel function is replaced by an outgoing spherical Hankel function); ν represents the spherical harmonic triple index (σ, m, n), where σ is e (even) or o (odd), n is the mode number, and m (in italics) is the azimuthal mode number; and the normalization constant is

$$D_\nu = \epsilon_m \frac{(2n+1)\,(n-m)!}{4n(n+1)(n+m)!}, \tag{2}$$

with $\epsilon_m = 1$ for $m = 0$, and $\epsilon_m = 2$ for $m > 0$.

The factors η_n^{TE} and η_n^{TM} become large when $x = ka$ = size parameter of the host sphere is that of a transverse electric (TE) or transverse magnetic (TM) resonance, respectively. They are

$$\eta_n^{TE} = \frac{i/\mathrm{m}x}{j_n(\mathrm{m}x)[xh_n^{(1)}(x)]' - [\mathrm{m}xj_n(\mathrm{m}x)]'h_n^{(1)}(x)} \tag{3}$$

and

$$\eta_n^{TM} = \frac{i/x}{\mathrm{m}^2 j_n(\mathrm{m}x)[xh_n^{(1)}(x)]' - [\mathrm{m}xj_n(\mathrm{m}x)]'h_n^{(1)}(x)}, \tag{4}$$

where $j_n(\mathrm{m}x)$ is the spherical Bessel function and $h_n^{(1)}(x)$ is the spherical Hankel function of the first kind. Derivatives (denoted by the primes) are with respect to their argument.

2.2 Calculation of the Image

The z-axis is chosen to be the line passing from the origin through the position of the dipole (see fig. 1). Therefore only the $m = 0$ and 1 azimuthal

*This Green function is obtained by rewriting equation A7 of S. C. Hill et al [25]; eliminating f_ν^G, g_ν^G, c_ν^H, and d_ν^H using equations A4, A5, A10, and A11; and eliminating the integral over source points.

modes are needed* in the expansion of the Green function (eq 1). There is no loss of generality, because the lens can be centered at any angle Θ and the dipole can be oriented in any direction.

The lens is centered on the z_{L_1}-axis of the lens coordinate system and on the z_{L_2}-axis of the L_2 coordinate system (whose origin is at the center of the sphere defined by S_2). The image plane is somewhere near the L_2 origin. We assume that the only nonzero fields on the surface enclosing the image plane are on S_2, over the region limited by the lens diameter.

Consider pairs of positions $\mathbf{r}_{S_1}$ and $\mathbf{r}_{S_2}$ (fig. 1), chosen so that the line joining them is parallel to the z_{L_1}- and z_{L_2}-axes. The field $\mathbf{E}(\mathbf{r}_{S_1})$ emitted from the dipole/sphere system is a diverging spherical wave on surface S_1 (with radius of curvature R_1; see fig. 1). The $\mathbf{E}(\mathbf{r}_{S_1})$ is converted by the diffraction-limited imaging system into a converging spherical wave $\mathbf{E}(\mathbf{r}_{S_2})$ on surface S_2 (with radius of curvature R_2). The $\mathbf{E}(\mathbf{r}_{S_1})$ are tangential to S_1 (because the lens is sufficiently distant from the sphere to be in the far field), and the $\mathbf{E}(\mathbf{r}_{S_2})$ are tangential to S_2. Then $E_\theta(\mathbf{r}_{S_2}) = E_\theta(\mathbf{r}_{S_1})$, and $E_\phi(\mathbf{r}_{S_2}) = -E_\phi(\mathbf{r}_{S_1})$. The image magnification (M) is the ratio of the radii of curvature, R_2/R_1.

Using Huygen's principle (vector Kirchhoff diffraction formula [29]), the electric field at image point $\mathbf{r}_I$ (not necessarily at nominal focus) is

$$\mathbf{E}(\mathbf{r}_I) = C \int_{S_2} \mathbf{E}(\mathbf{r}_{S_2}) \frac{\exp(ik|\mathbf{r}_I - \mathbf{r}_{S_2}|)}{|\mathbf{r}_I - \mathbf{r}_{S_2}|} \cos\left(\frac{-\mathbf{r}_{S_2}}{|\mathbf{r}_{S_2}|} \cdot \frac{(\mathbf{r}_I - \mathbf{r}_{S_2})}{|\mathbf{r}_I - \mathbf{r}_{S_2}|}\right) \mathrm{dA}, \quad (5)$$

where C is a constant, which we will ignore. The obliquity factor (the cosine term) can be ignored for the images we calculate here with NA = 0.5, because all the image points are sufficiently close to the z_{L_2}-axis that the minimum value of the obliquity factor for point on S_2 is 0.996 (and for most points is much closer to 1.0), and we have never observed it to have an effect on an image.

The intensity at $\mathbf{r}_I$, omitting a proportionality constant, is $I(\mathbf{r}_I) = |\mathbf{E}(\mathbf{r}_I)|^2$. The integral over S_2 is evaluated numerically. In integrating over frequency, the intensities of the images are weighted by the molecule's Lorentzian lineshape function.

Our method of calculation differs from approaches used previously for calculating elastic scattering images from particles [13,15–17], because we

*The advantage of choosing the z-axis to pass through the dipole, and thereby limiting the required m to 0 and 1, is that it provides a way to obtain images for relatively large spheres without computing the angular functions and coefficients for all m up to n (and without exceeding the available computer storage if these are saved). The disadvantage is that it requires more manipulation and coordinate transformations afterwards.

do not make the Fresnel approximation, but do calculate the vector fields in the image plane. Therefore our approach is not restricted to relatively small numerical apertures. In the previously calculated two-dimensional elastic scattering images [17] the NA was 0.024. It is not clear how much larger the NA could have been with the Fresnel approximation employed. However, it is unlikely that the Fresnel approximation with scalar fields would be adequate for calculating the large NA images obtained for single molecules in microparticles. In such experiments the NA is kept relatively large (e.g., 0.5) in order to increase the fraction of the light collected and to achieve a higher spatial resolution.

3. Results and Discussion

Figure 2 illustrates calculated images of a dipole near the surface (r/a = 0.9999) of a 5-μm-diameter sphere imaged with an NA 0.5 lens at $\Theta = 90°$ from the z-axis. (If the refractive index of the sphere is set to m = 1 for this case (not shown)—i.e., there is no sphere—a single bright spot appears near $x_{L_2}/aM = -1.0$, y_{L_2}/aM = 0 (for the x-polarized case it is a single bright ring), and its spot size, consistent with the diffraction limit, is comparable to those seen in fig. 2.) The emission at a nonresonant frequency (column 2) peaks near the edge of the sphere (near $x_{L_2}/Ma = \pm 1.0$ and y_{L_2}/Ma = 0) for all three polarizations (z- or radial in top row, x- in middle row, y- in bottom row). The peak of the emission at resonant frequencies (columns 3 and 4), as well as part of the frequency-integrated- (column 1) and nonresonant- (column 2) emission *appears* to originate outside the sphere, near $x_{L_2}/aM = \pm 1.3$, y_{L_2}/aM = 0. The appearance of on-resonance emission outside the sphere is consistent with the facts that (a) for MDRs having Qs such as these (10^4 to 2×10^4), the most efficient way to excite an MDR with a Gaussian beam is to focus the beam outside the sphere (r/a ~1.2 to 1.3) [30–33], and (b) the excitation and emission problems are related by reciprocity [34,35]. It is also consistent with previous calculations of glare spots in the on-resonance, 90° elastic scattering images of microspheres [17], in which one of the glare spots peaks outside the sphere, near r/a = 1.17. However, with a sphere on a surface [5], it is unlikely that this type of peaking of the emission outside the sphere will be observed if the mode volume overlaps appreciably with the planar surface, because the surface disturbs the fields and spoils the resonance. For the sphere-on-a-surface problem, MDRs whose near fields have less overlap with the surface might be chosen by measuring images in different directions with respect to the sphere/plane system.

This appearance of on-resonance emission outside the sphere does not require the molecule to be at the surface. When the emission frequencies are at a sphere resonance and when the dipole at the surface is oriented in a way that generates high-intensity spots in the image (e.g., row 2, column 3, or row 3, column 4) then the dipole can be taken further inside the sphere, to r/a as small as about 0.8, and the images appear almost identical (not shown) to images of the sphere on the surface, except that the overall intensity of the image depends on the dipole position (it scales as the squared modulus of the appropriate radial function at the position of the dipole $\mathbf{r}'$,

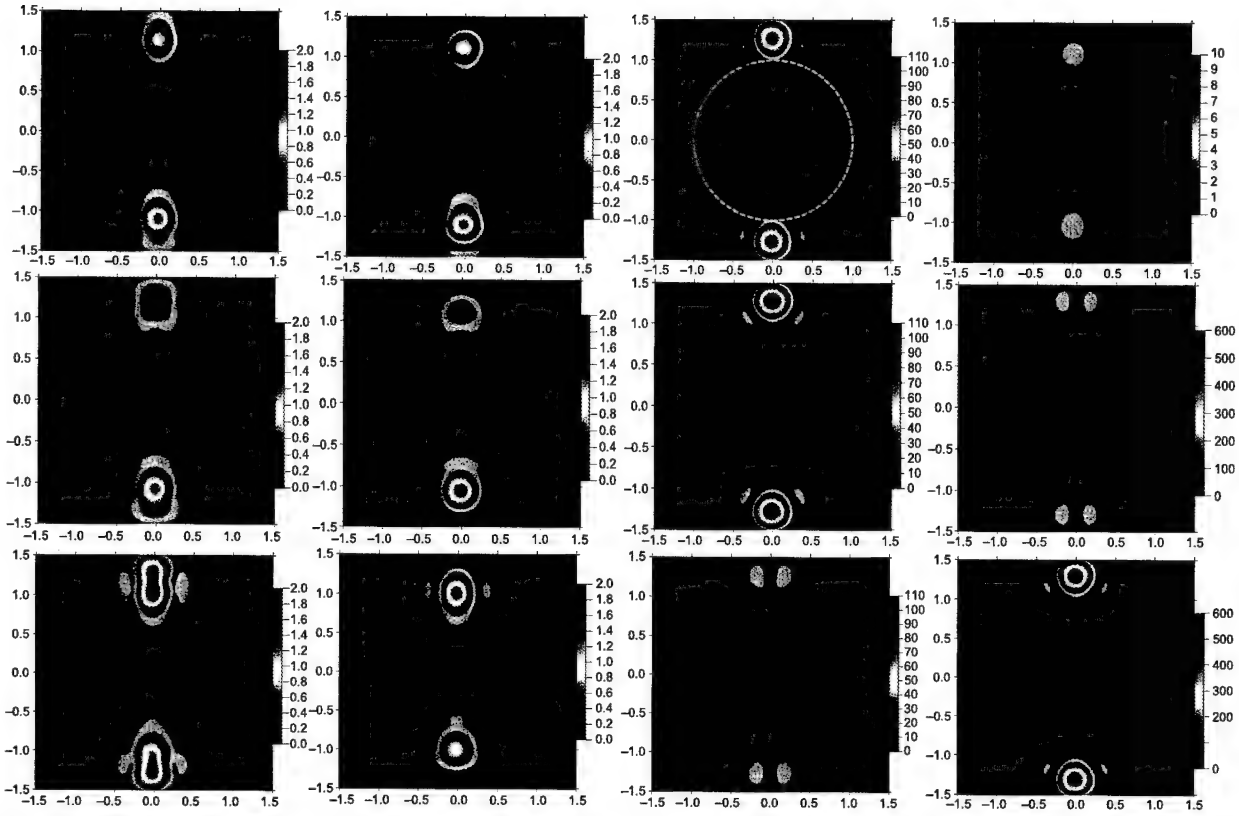

Figure 2. Calculated images of dipole at $r/a = 0.9999$ in 5-μm-diameter sphere of refractive index 1.454. Image plane is at origin of L_2 coordinate system. Horizontal axis is y_{L_2}/aM, and vertical axis is x_{L_2}/aM. Dotted line in top row, third column, shows where edge of sphere would be imaged in geometrical optics limit. Dipole is polarized in the z- (x_{L_2}-), x- (z_{L_2}-), and y- (y_{L_2}-) directions in top, middle, and bottom rows, respectively. In first column emission is integrated over frequency from 16367 cm^{-1} to 16967 cm^{-1} (encompassing 5 MDRs). Molecule's emission is centered at 16667 cm^{-1}, and it has Lorentzian linewidth (full width half maximum) of 100 cm^{-1}. In second column single-frequency emission is at 16666.7 cm^{-1}, which is not on resonance. In third column emission is on TM $_{32,1}$ MDR (16559.7851 cm^{-1}, with $Q = 10^4$). In fourth column emission is on TE$_{33,1}$ MDR (16742.035 cm^{-1} with $Q = 2.2 \times 10^4$). Maximum values of color scales have been adjusted to show main variations: with magnitude of dipole held constant, peak values are 2 in rows 1 and 2, 110 in row 3, and 600 in row 4 (except for top row of column 4, where it is only 10). Distance from center of sphere to plane of lens is 1 mm, and from plane of lens to image is 40 mm.

as expected from eq (1)). That is, emission from a dipole at $r/a = 0.8$ can appear to come from a dipole at $r/a = \pm 1.3$. As r/a decreases below about 0.8, the resonant contribution to the images decreases so that the nonresonant emission becomes more prominent and, for $r/a < 0.75$, dominates the image. For the TE$_{33}$ MDR with the y-polarized dipole (row 3, column 4), the maximum of the $j_{33}(mkr)$ occurs at $r/a = 0.948$ and the intensities in the image are about 2.2 times those for the dipole at the surface.

In the images at resonant frequencies (columns 3 and 4) the intensity is symmetrical about the planes defined by $x_{L_2} = 0$, and $y_{L_2} = 0$. In the non-

resonant images (column 2) the emission is asymmetrical about $x_{L_2} = 0$, and for y-polarization the emission is brighter on the side opposite where the dipole would be imaged if the sphere were not there. In column 1 (integrated over emission frequency) the images appear to be weighted superpositions of columns 2, 3, and 4 (the nonresonant and resonant emission). The weights are such that all three components (nonresonant, TE MDR, TM MDR) appear in different images. For the y-directed dipole (column 1) there are two intensity peaks on each side of the image, one near the sphere's surface and one outside it, and so it appears that the nonresonant and TE MDR contributions to the images are comparable. For the other dipole orientations the resonant modes contribute less than the nonresonant frequencies.

Figure 3 illustrates calculated images of a y-oriented dipole similar to those in the bottom row in figure 2, but with the lens at 165° from the z-axis. In the upper row the focus position is the same as that for figure 2 (it is set to image origin 1 to origin 2 when the sphere is not there). There are no sharply defined bright points. In the lower row the detector plane has been brought 10 mm closer to the lens, to decrease the spot size. This means that the detector plane is 6.5 mm closer to the lens than would be required for the dipole to be imaged to a small spot if the sphere were not there.* These calculations show that with the NA as large as 0.5, two dipoles in a 5-μm-diameter sphere may not be observed as two dipoles because one may be so out of focus that it appears only as diffuse light.

The images in figures 2 and 3 have at least one plane of symmetry ($y_{L_2} = 0$) because the dipole orientations are symmetric about the $y = 0$ plane. Figure 4 illustrates the type of nonsymmetric images that occur for dipoles not symmetric about $y = 0$. In each image the dipole's orientation is $\mathbf{i}_x + \mathbf{i}_y + \mathbf{i}_z$ (with the same total magnitude as in fig. 2 and 3). The dipole is at 135° from the lens center (left image) and 165° from the lens center (right image). The images are not symmetric. The image of the dipole at $\Theta = 135°$ appears to be only a perturbation from a symmetric case. However, the image of the dipole at $\Theta = 165°$ is highly asymmetric.

If the fluorescing molecules photobleach slowly, so that there is time to focus first on one molecule and then on another, then it should be possible to (a) experimentally distinguish the single- and multiple-dipole cases and (b) estimate from the focus positions where the molecules are. If the sphere can also be imaged from different directions, it may also be possible to use these results to determine the orientations of the dipoles.

*If $m = 1$ and $\Theta = 165°$, then with the lens law the image plane should be at $z_{L_2} = 3.52$ mm. The calculated images have spot sizes that do not vary markedly between $z_{L_2} = 2.5$ and 4.5 mm.

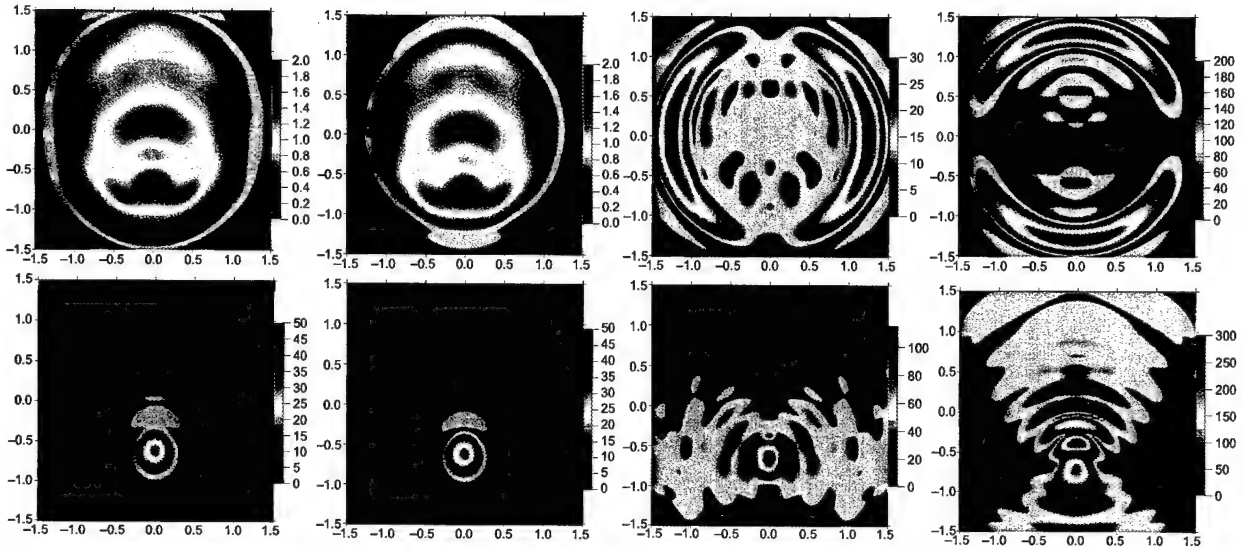

Figure 3. Calculated images of dipole in sphere as in figure 2, but with lens at $\Theta = 165°$ from z-axis. In upper row image plane is at origin of L_2 coordinate system. In lower row image plane is at $z_{L_2} = 10$ mm (i.e., 10 mm closer to lens than in fig. 2), so that the spot size is smaller.

Figure 4. Calculated images of dipole in sphere as in figure 2, except that dipole's polarization is $\mathbf{p}(\mathbf{r}') = (\mathbf{i}_x + \mathbf{i}_y + \mathbf{i}_z)/\sqrt{3}$, and lens is at $\Theta = 135°$ (left image) and $\Theta = 165°$ (right image). Images are integrated over emission frequency with same parameters as in figure 2.

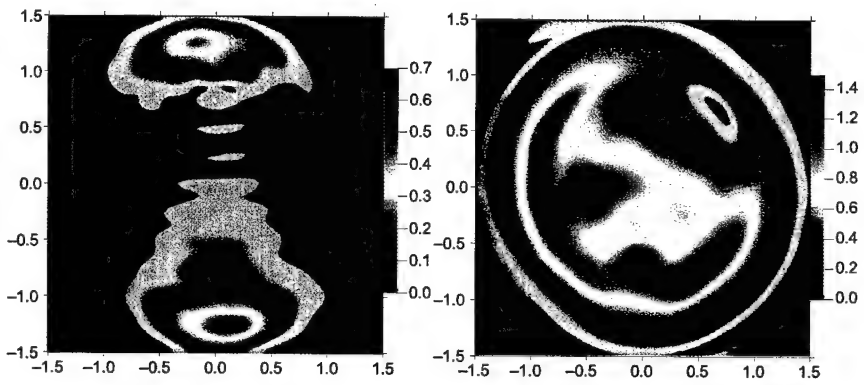

4. Conclusions

We modeled fluorescence images of single molecules in microspheres, and demonstrated how the images depend on the position, orientation, and emission frequencies of the molecule. One result is surprising, at least at first glance: when the dipole's emission frequency coincides with a resonance frequency of the microsphere, the brightest regions in the images occur outside the boundary of the sphere, at r/a in the range of 1.2 to 1.3, for some dipole positions. This observation is similar to calculations and measurements of the excitation of sphere resonances with Gaussian beams focused outside of a sphere. However, the two cases are different in that the emission from the dipole is more symmetrical and lacks the focus of the Gaussian beam. As far as we know, experimental images with the emission appearing to peak outside the sphere when the sphere is in focus have not been reported.

Calculations of the type presented here may help in interpreting images of molecules in microspheres and in suggesting useful experimental arrangements for determining the positions and orientations of single molecules in microspheres.

This work was sponsored in part by the U.S. Department of Energy, Office of Basic Energy Sciences, Oak Ridge National Laboratory, including contract DE-AC05-96OR22464 to the U.S. Army Research Laboratory.

References

1. R. M. Dickson, D. J. Norris, Y.-L. Tzeng, and W. E. Moerner, "Three-dimensional imaging of single molecules solvated in pores of poly(acrylamide) gels," Science **274**, 966–969 (1996).

2. J. J. Macklin, J. K. Trautman, T. D. Harris, and L. E. Brus, "Imaging and time-resolved spectroscopy of single molecules at an interface," Science **272**, 255–258 (1996).

3. W. E. Moerner and M. Orrit, "Illuminating single molecules in condensed matter," Science **283**, 1670–1676 (1999).

4. D. J. Norris, M. Kuwata-Gonokami, and W. E. Moerner, "Excitation of a single molecule on the surface of a spherical microcavity," Appl. Phys. Lett. **71**, 297–299 (1997).

5. M. D. Barnes, K. C. Ng, K. P. McNamara, C.-Y. Kung, J. M. Ramsey, and S. C. Hill, "Fluorescence imaging of single molecules in polymer microspheres," Cytometry, in press.

6. S.-X. Qian, J. B. Snow, H.-M. Tzeng, and R. K. Chang, "Lasing droplets: highlighting the liquid-air interface by laser emission," Science **231**, 486–488 (1986).

7. J.-Z. Zhang, G. Chen, and R. K. Chang, "Pumping of stimulated Raman scattering by stimulated Brillouin scattering within a single liquid droplet: input laser linewidth effects," J. Opt. Soc. Am. B **7**, 108–115 (1990).

8. S. Arnold and L. M. Folan, "Microphotography of an electrodynamically levitated particle," Proc. SPIE **1862**, 218–222 (1993).

9. S. Arnold, S. Holler, and S. D. Druger, "Imaging enhanced energy transfer in a levitated aerosol particle," J. Chem. Phys. **104**, 7741–7748 (1996).

10. M. Winter and L. A. Melton, "Measurement of internal circulation in droplets using laser-induced fluorescence," Appl. Opt. **29**, 4574–4577 (1990).

11. S. R. Harris, W. R. Lempert, L. Hersch, C. L. Burcham, D. A. Saville, and R. B. Miles, "Quantitative measurements of internal circulation in droplets using flow tagging velocimetry," AIAA J. **34**, 449–454 (1996).

12. M. D. Barnes, C.-Y. Kung, W. B. Whitten, J. M. Ramsey, S. Arnold, and S. Holler, "Fluorescence of oriented molecules in a microcavity," Phys. Rev. Lett. **76**, 3931–3934 (1996).

13. J. A. Lock, "Theory of the observations made of high-order rainbows from a single water droplet," Appl. Opt. **26**, 5291–5298 (1987).

14. H. C. van de Hulst and R. T. Wang, "Glare points," Appl. Opt. **30**, 4755–4763 (1991).

15. S. A. Schaub, D. R. Alexander, and J. P. Barton, "Theoretical model of the laser imaging of small aerosols: applications to aerosol sizing," Appl. Opt. **30**, 4777–4784 (1991).

16. S. Arnold, S. Holler, J. H. Li, A. Serpenguzel, W. F. Auffermann, and S. C. Hill, "Aerosol particle microphotography and glare-spot absorption spectroscopy," Opt. Lett. **20**, 773–775 (1995).

17. S. A. Schaub, D. R. Alexander, and J. P. Barton, "Glare spot image calculations for a spherical particle illuminated by a tightly focused beam," J. Opt. Soc. Am. A **9**, 316–330 (1992).

18. J. Zhang and L. A. Melton, "Numerical simulations and restorations of laser droplet-slicing images," Appl. Opt. **334**, 192–200 (1990).

19. R. K. Chang and A. J. Campillo, *Optical Processes in Microcavities* (World Scientific, Singapore, 1996).

20. M. D. Barnes, W. B. Whitten, S. Arnold, and J. M. Ramsey, "Homogeneous linewidths of rhodamine 6G at room temperature from cavity enhanced spontaneous emission rates," J. Chem. Phys. **97**, 7842–7845 (1992).

21. H.-B. Lin, J. D. Eversole, C. D. Merrit, and A. J. Campillo, "Cavity-modified spontaneous emission rates in liquid microdroplets," Phys. Rev. A **45**, 6756 (1992).

22. N. Lermer, M. D. Barnes, C.-Y. Kung, W. B. Whitten, J. M. Ramsey, and S. C. Hill, "Spatial photoselection of single molecules on the surface of a spherical microcavity," Opt. Lett. **23**, 951–953 (1998).

23. C.-Y. Kung, M. D. Barnes, N. Lermer, W. B. Whitten, and J. M. Ramsey, "Single molecule analysis of ultradilute solutions with guided streams of 1-μm water droplets," Appl. Opt. **38**, 1481–1487 (1999).

24. H. Chew, P. J. McNulty, and M. Kerker, "Model for Raman and fluorescent scattering by molecules embedded in small particles," Phys. Rev. A. **13**, 396–404 (1976).

25. S. C. Hill, H. I. Saleheen, M. D. Barnes, W. B. Whitten, and J. M. Ramsey, "Modeling fluorescence collection from single molecules in microspheres: Effects of position, orientation, and frequency," Appl. Opt. **35**, 6278–6288 (1996).

26. J. W. Goodman, *Introduction to Fourier Optics*, 2nd ed. (McGraw-Hill, New York, 1998), 128.

27. C. R. Bohren and D. R. Huffman, *Absorption and Scattering of Light by Small Particles* (Wiley, New York, 1983), 89.

28. P. W. Barber and S. C. Hill, *Light Scattering by Particles: Computational Methods* (World Scientific, Singapore, 1990), 84.

29. J. D. Jackson, *Classical Electrodynamics*, 3rd ed. (Wiley, New York, 1999), 484.

30. J. P. Barton, D. R. Alexander, and S. A. Schaub, "Internal fields of a spherical particle illuminated by a tightly focused laser beam: Focal point positioning effects at resonance," J. Appl. Phys. **65**, 2900–2906 (1989).

31. E.E.M. Khaled, S. C. Hill, P. W. Barber, and D. Q. Chowdhury, "Near-resonance excitation of morphology dependent resonances with plane waves and off-axis Gaussian beams," Appl. Opt. **31**, 1166–1169 (1992).

32. J. A. Lock, "Excitation efficiency of a morphology-dependent resonance by a focused Gaussian beam," J. Opt. Soc. Am. A **15**, 2986–2994 (1998).

33. H.-B. Lin, J. D. Eversole, A. J. Campillo, and J. P. Barton, "Excitation localization principle for spherical microcavities," Opt. Lett. **23**, 1921–1923 (1998).

34. S. C. Hill, G. Videen, and J. D. Pendleton, "Reciprocity method for obtaining the far fields generated by a source inside or near a scattering object," J. Opt. Soc. Am. B **14**, 2522–2529 (1997).

35. N. Velesco and G. Schweiger, "Geometrical optics calculation of inelastic scattering on large particles," Appl. Opt. **38**, 1046–1052 (1999).

Distribution

Admnstr
Defns Techl Info Ctr
Attn DTIC-OCP
8725 John J Kingman Rd Ste 0944
FT Belvoir VA 22060-6218

Central Intllgnc Agency
Dir DB Standard
Attn GE 47 QB
Washington DC 20505

Chairman Joint Chiefs of Staff
Attn J5 R&D Div
Washington DC 20301

Dir of Defns Rsrch & Engrg
Attn DD TWP
Attn Engrg
Washington DC 20301

Ofc of the Secy of Defns
Attn ODDRE (R&AT)
The Pentagon
Washington DC 20301-3080

OSD
Attn OUSD(A&T)/ODDR&E(R) R J Trew
Washington DC 20301-7100

Commanding Officer
Attn NMCB23
6205 Stuart Rd Ste 101
FT Belvoir VA 22060-5275

AMCOM MRDEC
Attn AMSMI-RD W C McCorkle
Redstone Arsenal AL 35898-5240

CECOM
Attn PM GPS COL S Young
FT Monmouth NJ 07703

Dir for MANPRINT
Ofc of the Deputy Chief of Staff for Prsnnl
Attn J Hiller
The Pentagon Rm 2C733
Washington DC 20301-0300

Dir of Chem & Nuc Ops DA DCSOPS
Attn Techl Lib
Washington DC 20301

US Army Armament Rsrch Dev & Engrg Ctr
Attn AMSTA-AR-TD M Fisette
Bldg 1
Picatinny Arsenal NJ 07806-5000

US Army Edgewood RDEC
Attn SCBRD-TD G Resnick
Aberdeen Proving Ground MD 21010-5423

US Army Engrg Div
Attn HNDED FD
PO Box 1500
Huntsville AL 35807

US Army Info Sys Engrg Cmnd
Attn ASQB-OTD F Jenia
FT Huachuca AZ 85613-5300

US Army Natick RDEC Acting Techl Dir
Attn SSCNC-T P Brandler
Natick MA 01760-5002

Director
US Army Rsrch Ofc
4300 S Miami Blvd
Research Triangle Park NC 27709

US Army Simulation, Train, & Instrmntn Cmnd
Attn J Stahl
12350 Research Parkway
Orlando FL 32826-3726

US Army Tank-Automtv Cmnd Rsrch, Dev, & Engrg Ctr
Attn AMSTA-TA J Chapin
Warren MI 48397-5000

US Army Train & Doctrine Cmnd Battle Lab Integration & Techl Dirctrt
Attn ATCD-B J A Klevecz
FT Monroe VA 23651-5850

Distribution (cont'd)

Nav Surface Warfare Ctr
Attn Code B07 J Pennella
17320 Dahlgren Rd Bldg 1470 Rm 1101
Dahlgren VA 22448-5100

DARPA
Attn B Kaspar
3701 N Fairfax Dr
Arlington VA 22203-1714

Hicks & Associates Inc
Attn G Singley III
1710 Goodrich Dr Ste 1300
McLean VA 22102

US Army ERDEC
Attn SCBRD-RTE I Sindoni
Attn SCBRD-RTE J Embury
Attn SCBRD-RTE M Milham
Attn SCBRD-RTE S Christesen

US Army ERDEC (cont'd)
Attn AMSCB-AL B Bronk
Attn SCBRD-RTE E Stuebing
Attn SCBRD-RTE J R Bottiger
Attn SCBRD-RTE R Smardzewski
Aberdeen Proving Ground MD 21005-5423

US Army Rsrch Lab
Attn AMSRL-DD J Rocchio
Attn AMSRL-CI-LL Techl Lib (3 copies)
Attn AMSRL-CS-AS Mail & Records Mgmt
Attn AMSRL-CS-EA-TP Techl Pub (3 copies)
Attn AMSRL-IS-EM S Hill (20 copies)
Attn AMSRL-IS-EM D Garvey
Adelphi MD 20783-1197

REPORT DOCUMENTATION PAGE

Form Approved
OMB No. 0704-0188

1. AGENCY USE ONLY *(Leave blank)*	2. REPORT DATE	3. REPORT TYPE AND DATES COVERED
	July 1999	May 1995 to March 1999

4. TITLE AND SUBTITLE Fluorescence Image of a Single Molecule in a Microsphere: Model

5. FUNDING NUMBERS
DA PR: B53A
PE: 61102A

6. AUTHOR(S) Steven C. Hill (ARL), Paul Nachman (TRW, Inc.), Stephen Arnold (Microparticle Photophysics Laboratory), J. Michael Ramsey and Michael D. Barnes (Oak Ridge National Laboratory)

7. PERFORMING ORGANIZATION NAME(S) AND ADDRESS(ES)
U.S. Army Research Laboratory
Attn: AMSRL- IS-EM email: shill@arl.mil
2800 Powder Mill Road
Adelphi, MD 20783-1197

8. PERFORMING ORGANIZATION REPORT NUMBER
ARL-TR-1979

9. SPONSORING/MONITORING AGENCY NAME(S) AND ADDRESS(ES)
Oak Ridge National Laboratory
Oak Ridge, TN 37831-6142

10. SPONSORING/MONITORING AGENCY REPORT NUMBER

11. SUPPLEMENTARY NOTES
ARL PR: 9FEJ71
AMS code: 61110253A11
This work has been accepted for publication in the Journal of the Optical Society of America B.

12a. DISTRIBUTION/AVAILABILITY STATEMENT
Approved for public release; distribution unlimited.

12b. DISTRIBUTION CODE

13. ABSTRACT *(Maximum 200 words)*
We model fluorescence images of single molecules in spherical dielectric microcavities. Molecules are treated as time-harmonic dipoles. Images are integrated over emission frequencies. Because of the strong refractive properties of the enclosing sphere, the fluorescence image depends on the refractive index of the sphere and the position, orientation, and emission frequency of the molecule. When the dipole's emission is at the frequency of a microsphere resonance, the brightest regions in the images appear to originate from outside the sphere for some dipole positions. This type of calculation should help in interpreting images of molecules in microspheres.

14. SUBJECT TERMS
fluorescence, particles, single molecules, microscopy

15. NUMBER OF PAGES
24

16. PRICE CODE

17. SECURITY CLASSIFICATION OF REPORT	18. SECURITY CLASSIFICATION OF THIS PAGE	19. SECURITY CLASSIFICATION OF ABSTRACT	20. LIMITATION OF ABSTRACT
Unclassified	Unclassified	Unclassified	UL

NSN 7540-01-280-5500

Standard Form 298 (Rev. 2-89)
Prescribed by ANSI Std. Z39-18
298-102